Molecular Crystals and Liquid Crystals
Publication details, including instructions for authors and subscription information:
http://www.tandfonline.com/loi/gmcl16

Measurement of Director Orientation at the Nematic—Isotropic Interface Using a Substrate-Nucleated Nematic Film

H. Yokoyama [a] , S. Kobayashi [a] & H. Kamei [a]
[a] Electrotechnical Laboratory, 1-1-4 Umezono, Sakura-mura, Niihari-gun, Ibaraki, 305, Japan
Version of record first published: 20 Apr 2011.

To cite this article: H. Yokoyama , S. Kobayashi & H. Kamei (1984): Measurement of Director Orientation at the Nematic—Isotropic Interface Using a Substrate-Nucleated Nematic Film, Molecular Crystals and Liquid Crystals, 107:3-4, 311-331

To link to this article: http://dx.doi.org/10.1080/00268948408070444

Mol. Cryst. Liq. Cryst., 1984, Vol. 107, pp. 311–331
0026-8941/84/1074–0311/$18.50/0

Printed in the United States of America

Measurement of Director Orientation at the Nematic–Isotropic Interface Using a Substrate-Nucleated Nematic Film

H. YOKOYAMA, S. KOBAYASHI and H. KAMEI

Electrotechnical Laboratory, 1-1-4 Umezono, Sakura-mura, Niihari-gun, Ibaraki 305 Japan

(*Received September 6, 1983*)

A flat and stable interface between the nematic and isotropic phases was prepared in a sandwich-type cell under thermal equilibrium conditions to determine the director orientation at the nematic–isotropic interface. The preparation method is based on the fact that a rubbed polyvinylalcohol film nucleates a surface nematic film when the isotropic liquid of a nematogen containing a small amount of impurity is cooled down passing through the clearing point. The impurity causes the nematic and isotropic phases to coexist over a finite temperature range in which the nucleated nematic film keeps its interface between the isotropic phase parallel to the substrate. Using the nematic–isotropic interface obtained this way, we determined the preferred orientation at the interface for a nematogen, 4-cyano-4′-*n*-pentylbiphenyl, mixed with a small amount of hexamethylbenzene, by observing the electric field-induced deformations in the nematic layer. For this purpose, a simple procedure which requires little knowledge about the material constants was developed theoretically. The director was found to be tilted by $28.1 \pm 0.6°$ from the interface, and its anchoring energy, or equivalently the anisotropy of the interfacial tension, was estimated to be on the order of 10^{-3} erg/cm^2.

I. INTRODUCTION

The nematic–isotropic interface is of particular interest among various interfaces involving nematic liquid crystals, in that it appears as a result of the first order nematic–isotropic transition and thus its properties are expected to be intimately related to the molecular

processes which give rise to the nematic order.[1] Despite its importance, only a few experimental efforts have been devoted to the nematic–isotropic interface up to now. This seems to stem from the difficulty associated with the preparation of a stable nematic–isotropic interface in an equilibrium condition. For this reason, all the experiments reported so far were more or less performed in thermal inequilibrium circumstances. The first experimental study on the nematic–isotropic interface was performed by Meyer[2] with a view to observing point disclinations at the interface, in which he made use of a temperature gradient through the sample to form the interface. Langevin and Bouchiat[3] also obtained the nematic–isotropic interface of MBBA (4-methoxybenzylidene-4′-*n*-butylaniline) in a temperature gradient. Observing light reflection and scattering from the interface, they found the director of the liquid crystal being parallel to the interface and estimated the interfacial tension. Williams[4] measured the interfacial tension for MBBA by the sessile drop method in good agreement with Langevin and Bouchiat's result and also with the value calculated theoretically by Sheng and Priestley.[5] On the other hand, Vilanove and co-workers[6] reported that for MBBA the director is conical, not parallel to the nematic–isotropic interface.

In this paper we employ a rather different approach toward the preparation of a stable nematic–isotropic interface. The method is based on the fact that if the gravitational effect can be neglected, the equilibrium configuration of two immiscible phases coexisting on a substrate is essentially determined by how the substrate is wetted by those phases. Specifically, if one of the substrates of a sandwich-type cell is completely wetted by the nematic phase and the other by the isotropic phase, we obtain a stratified configuration of the nematic and isotropic layers with their interface parallel to the substrates. This condition can, at least approximately, be achieved by properly treating the substrate surfaces, as reported previously.[7,8] This technique, when compared with the temperature gradient method, has an obvious advantage that the nematic–isotropic interface can be obtained in a conventional sandwich-type cell under thermal equilibrium conditions. In the next section, the details of the preparation are given. As an application of the nematic–isotropic interface thus obtained, we measured the director orientation at the interface by observing the electric field-induced deformations of the director in the nematic layer. The theory of the measurement is described in Section III, and Section IV is devoted to results and discussion. Finally the conclusion is given in Section V.

II. PREPARATION OF THE NEMATIC–ISOTROPIC INTERFACE

The coexistence of the nematic and isotropic phases is obviously the prerequisite for the preparation of the nematic–isotropic interface. In a pure material, this occurs only at the clearing temperature, and therefore a slight change in temperature is enough to make observations impossible. In order to avoid this, we incorporate a small amount of impurity into the liquid crystal to give a finite temperature range over which the nematic and isotropic phases coexist in equilibrium. Figure 1 shows the phase diagram for such a mixture; hexamethylbenzene, $C_6(CH_3)_6$, in 4-cyano-4′-*n*-pentylbiphenyl(5CB). When the mixture is cooled down from the isotropic phase, the nematic phase first appears at the temperature, T_i, and grows until the isotropic phase finally disappears at T_n. The relative amounts of the nematic and isotropic phases in the coexistence region can be determined by the "lever law".[9] It should, thus, be stressed that the nematic–isotropic interface of a mixture is always accompanied by the concentration as well as the order parameter variations. However, there are

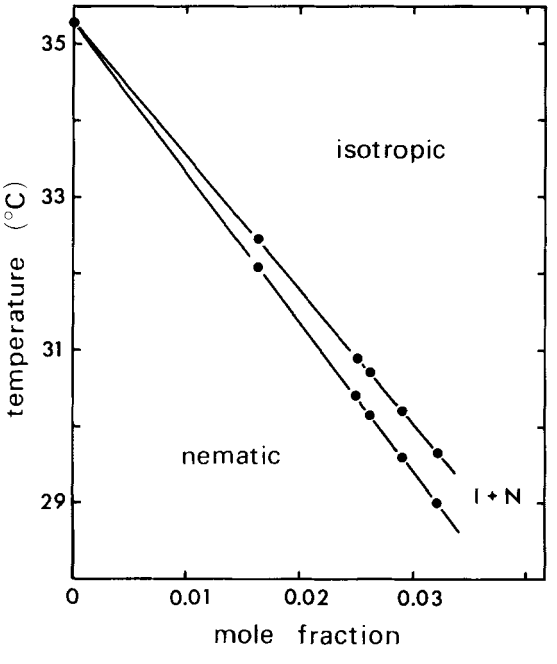

FIGURE 1 Phase diagram for $C_6(CH_3)_6$/5CB.

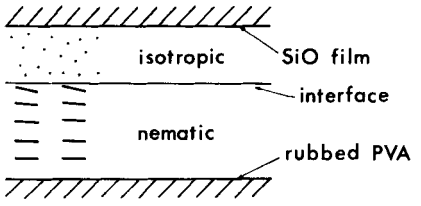

FIGURE 2 Equilibrium configuration of coexisting nematic and isotropic phases sandwiched between properly treated substrates.

several theoretical and experimental evidences which indicate that the physical properties of a liquid crystal mixture in or near the nematic–isotropic coexistence region are approximately independent of the concentration of the impurity molecules as far as the mixture can be considered dilute.[10–12] So we can expect that a study on the nematic–isotropic interface of a mixture will also give close insights into the interfacial properties of a pure material.

As already mentioned, the present method relies on the control of the wettability of substrates to the nematic and isotropic phases by applying proper surface treatments so that one substrate is wetted by the nematic phase and the other by the isotropic phase (Figure 2). The appropriate surface treatments and their procedures are listed in Table 1. Glass slides having a transparent electrode (indium tin oxide) were used as a substrate. The treated substrates were mutually oriented so as to align the liquid crystal homogeneously in the nematic phase. A sandwich-type cell was constructed with 40-μm-thick polyester film spacer, and its actual thickness was determined to be 43 μm from the

TABLE I

Relevant surface treatments and their procedures

Surface treatment	Procedure	Wetting characteristic
Coating with rubbed PVA film	A glass slide is spin coated with a 1 wt% aqueous solution of PVA and dried at 80 °C for 5 h, and then rubbed with lens cleaning paper.	Well wetted by the nematic phase
Oblique evaporation of SiO	SiO is evaporated at 60 ° from the substrate normal in vacuum of 10^{-6} torr at the rate of 7 Å/s for 90 s.	Well wetted by the isotropic phase

interference spectrum. Then the cell was injected with 2.6 mol% mixture of 5CB and $C_6(CH_3)_6$.

The cell was placed in a home-built polarizing microscope in which the sample temperature can be controlled with 10^{-3}°C accuracy.[13] The sample was illuminated by a collimated monochromatic light (wavelength = 560 nm) between crossed polarizers, the axes of which were inclined from the optic axis of the liquid crystal by 45°. Besides usual microscopic observations, the transmitted light intensity, I_t, was simultaneously monitored through the microscope, in order to quantitatively evaluate the optical phase difference, δ, caused by the nematic liquid;

$$I_t \propto \sin^2(\pi\delta). \tag{1}$$

On cooling from the isotropic phase, the rubbed PVA (polyvinylalcohol) film nucleated a surface film of nematic phase at T_i = 30.73°C. Although the surface film was mostly uniform in its thickness, a number of defects were also observed at the beginning. As the thickness increased, the nematic liquid rapidly invaded the defects, and usually consumed them until the thickness reached a few micrometers. Once the defects disappeared, the nematic film became so uniform that no birefringence fringe pattern could be observed over the field of view (700 μm in diameter). This uniform nematic layer was quite stable and we could reversibly change its thickness in a relatively wide range by controlling the temperature.

The inset of Figure 3 shows the time variation of the transmitted light intensity, when the temperature was decreased at the rate of 0.58°C/h through the coexistence region. In view of Eq. (1) and the above microscopic observations, the oscillation of the transmitted light intensity can be attributed to the increase of δ due to the growth of the nematic layer. The intensity oscillates about eight times before the nematic layer reaches the upper substrate. So we can roughly say that as one moves in the field of view of a microscope from a certain birefringence fringe to the neighboring one, the nematic layer changes its thickness by about 5 μm. Therefore, we can estimate the angle of inclination of the nematic–isotropic interface to be less than 0.4° with respect to the substrate surface.

When the temperature approached the lower boundary of the coexistence region and the interface came up to one or two micrometers from the SiO evaporated substrate, the uniformity of the layer was a bit disturbed due probably to dust particles on the substrate. On further cooling, the nematic layer made direct contact with the SiO

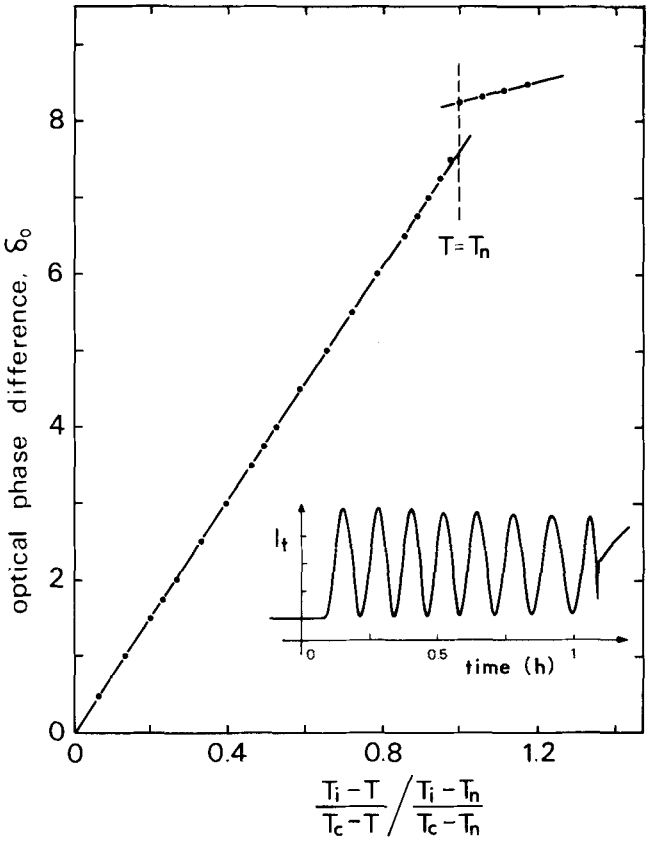

FIGURE 3 *Temperature dependence of the optical phase difference, δ_0, through the nematic–isotropic coexistence region when the temperature was lowered at 0.58 °C/h. T_i (= 30.73 °C) and T_n (= 30.15 °C) are the upper and the lower boundaries of the coexistence region, respectively. T_c (= 35.3 °C) is the clearing temperature of pure 5CB. The inset shows the time variation of the transmitted light intensity from which δ_0 was deduced.*

film, leaving little amount of isotropic liquid at the interface. As a result, the homogeneous alignment was regained immediately. The lower boundary of the coexistence region, T_n = 30.15 °C, was determined as the temperature at which the isotropic liquid disappeared completely from the field of view. When the cell was heated from the nematic phase, the isotropic liquid was first nucleated about 0.005 °C above T_n at the SiO film-liquid crystal interface. This very weak super heating may be a consequence of the small contact angle of the isotropic liquid at this interface.[8]

The behavior described above is not specific to the mixture used here. We have actually observed a same type of behavior for MBBA. In what follows, however, we restrict the attention to the case of 5CB, because it is readily amenable to an electric field when homogeneously aligned.

In order to perform quantitative measurements as well as to evaluate the nematic layer itself, the precise knowledge about the layer thickness is fundamental. As is clear from above, the optical phase difference, δ, can be used as a measure for the thickness. If we assume the director to be homogeneously oriented throughout the nematic layer, the optical phase difference can be written as

$$\delta = d(n_e - n_o)/\lambda \tag{2}$$

where d is the thickness, λ is the wavelength of light, and n_e and n_o are, respectively, the refractive indices for extraordinary and ordinary rays. As already mentioned, we have a good reason to believe that material parameters such as refractive indices are constant through the coexistence region. So, in this case, δ is strictly proportional to the thickness of the nematic layer. But, in reality, the director is not necessarily uniform in the layer. In most practical conditions, however, we can show that δ is still proportional to the layer thickness to a good approximation. This point will be returned shortly in the following section.

When the nematic and isotropic layers are in thermal equilibrium, the relative amounts, therefore the relative thickness, of the two phases can also be derived from the phase diagram (Figure 1). According to the lever law, the thickness of the nematic layer at T ($T_n < T < T_i$) is proportional to

$$(T_i - T)/(T_c - T) \tag{3}$$

where T_c ($= 35.3°C$) is the clearing temperature of pure 5CB. In deriving Eq. (3), the small volume change at the transition is neglected, and use is made of the fact that the phase boundaries of the coexistence region are well approximated by straight lines intersecting at T_c. In Figure 3, the optical phase difference is plotted against Eq. (3) normalized at T_n. As expected, the linearity between δ and $(T_i - T)/(T_c - T)$ is very good except very near $T = T_n$ where the planar nematic–isotropic interface became unstable. This confirms again that the stratified configuration of the nematic and isotropic phases is a direct consequence of the equilibrium phase separation of the mixture.

The variation of δ below T_n should of course be attributed to the increase in the birefringence of the liquid crystal. Here, it must be emphasized that at T_n there exists a discontinuous rise in the optical phase difference, implying the presence of director tilt at the nematic–isotropic interface. In Figure 3, extrapolating δ to T_n from the lower and the higher temperature sides give 8.25 and 7.58, respectively. It is now widely accepted that a director tilt at confining walls affects the elastic deformations drastically in an external field.[14] In the rest of this paper, we shall attempt to determine the director orientation at the nematic–isotropic interface by observing the elastic deformations in an electric field.

III. THEORY OF THE TILT ANGLE DETERMINATION

The director deformations in an electric field can be in general calculated under any boundary conditions, when the material parameters such as elastic and dielectric constants are known. Therefore, by comparing the theoretical and experimental results, we can in principle obtain the director orientations imposed at the confining walls.[15] At present, however, we can find a simpler procedure to determine the tilt angle which requires little explicit knowledge about the material parameters.

In order to illustrate the method, let us first consider a slab of a nematic liquid crystal of positive dielectric anisotropy confined between two different types of substrates (see Figure 4). One of the substrates is assumed to align the liquid crystal homogeneously with infinite strength, and the other to give a conical boundary condition degenerate with respect to the rotation about the substrate normal. Consequently, only the contribution from the upper substrate to the total free energy needs to be considered explicitly. We write it as $F(\theta_i, \theta_t)$, where θ_i is the actual angle between the director and the

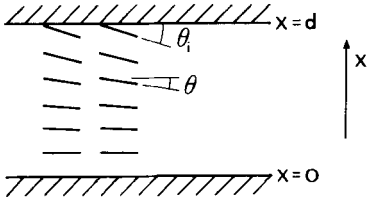

FIGURE 4 Illustration of the geometry. The director is homogeneously anchored at the lower substrate ($x = 0$), but is tilted at the upper substrate ($x = d$).

substrate and θ_t is the angle of the director at which the interfacial free energy takes the minimum value (referred to as the tilt angle, here). With the variables defined in Figure 4, the total free energy per unit area of the nematic slab can be written as a sum of the elastic energy, the dielectric energy and the interfacial free energy;

$$\int_0^d \frac{1}{2}\left(K_1\cos^2\theta + K_3\sin^2\theta\right)\left(\frac{d\theta}{dx}\right)^2 + \frac{1}{2}\mathbf{D}\cdot\mathbf{E}\,dx + F(\theta_i, \theta_t) \quad (4)$$

where K_1 and K_3 are the elastic constants for splay and bend deformations, and **E** and **D** are the electric field and the electric displacement, respectively. The equilibrium distributions of the director can be found by minimizing the total free energy with respect to θ under the constraint of constant charges on external conductors. Since **D** satisfies $\mathrm{div}\,\mathbf{D} = 0$, the x-component of **D**, D_x, is uniform throughout the sample. By applying the variational calculus to Eq. (4), we obtain the Euler-Lagrange equation;

$$\frac{d}{dx}\left\{\left(K_1\cos^2\theta + K_3\sin^2\theta\right)\left(\frac{d\theta}{dx}\right)^2 - \frac{D_x^2}{\epsilon_2\epsilon_0}\left(1 + \frac{\Delta\epsilon}{\epsilon_2}\sin^2\theta\right)^{-1}\right\} = 0,$$

$$\Delta\epsilon = \epsilon_1 - \epsilon_2 \quad (5)$$

with boundary conditions,

$$\theta = 0 \qquad \text{at } x = 0,$$

$$\left(K_1\cos^2\theta_i + K_3\sin^2\theta_i\right)\frac{d\theta}{dx} = -\frac{d}{d\theta_i}F(\theta_i, \theta_t) \qquad \text{at } x = d \quad (6)$$

where ϵ_1 and ϵ_2 are, respectively, the dielectric constants in the directions parallel and perpendicular to the director. The optical phase difference, δ, can be written as an implicit function of the applied voltage, V, through the director field, $\theta(x)$;

$$\delta = \frac{1}{\lambda}\int_0^d n_{ef}(\theta) - n_o\,dx,$$

$$n_{ef}(\theta) = \left(\frac{\sin^2\theta}{n_o^2} + \frac{\cos^2\theta}{n_e^2}\right)^{-1/2}, \quad (7)$$

$$V = \frac{D_x}{\epsilon_2\epsilon_0}\int_0^d\left(1 + \frac{\Delta\epsilon}{\epsilon_2}\sin^2\theta\right)^{-1} dx. \quad (8)$$

These equations constitute the basis of our present analysis.

Generally speaking, due to the incomplete anchoring at the boundary, θ_i may differ from the "intrinsic" tilt angle, θ_t. In fact, as the voltage is increased from zero, θ_i also increases passing through θ_t at a certain voltage, say, V_t. How θ_i changes with the voltage is obviously dependent not only on the value of θ_t but on the behavior of $F(\theta_i, \theta_t)$ around $\theta_i = \theta_t$. Our primary concern, here, is to find the tilt angle, θ_t. Since Eq. (6) involves only the derivative of $F(\theta_i, \theta_t)$ which vanishes at $\theta_i = \theta_t$ from the definition of θ_t, it is clear that the director configuration at $V = V_t$ is determined only by the value of θ_t. So, at this point, the voltage as well as the optical phase difference must be independent of the anchoring strength at the upper boundary. This situation is illustrated in Figure 5 by numerically calculating the optical phase difference as a function of voltage for various anchoring strengths. In the calculation, we assumed $\frac{1}{2}E_a\sin^2(\theta_i - \theta_t)$ for $F(\theta_i, \theta_t)$. It is clear that all the curves intersect at the same point irrespective of the values of E_a. Therefore, if we can find the intersection point

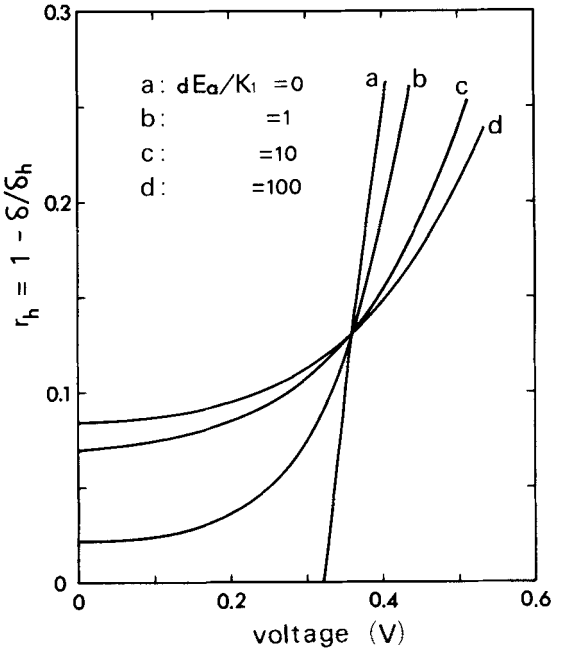

FIGURE 5 The calculated r_h vs V curves for various anchoring strengths. δ: optical phase difference. $\delta_h = d(n_e - n_o)/\lambda$, $\epsilon_2 = \Delta\epsilon = 8$, $n_e = 1.6$, $n_o = 1.5$, $\lambda = 560$ nm, $d = 30\ \mu$m, $\theta_t = 0.5$, $K_1 = K_3 = 3 \times 10^{-7}$ dyn.

experimentally and have some means to relate it with the tilt angle, we can determine the tilt angle without knowing the anchoring strength.

In order to obtain the optical phase difference and the voltage at the intersection as a function of θ_t, let us consider the case of $F(\theta_i, \theta_t) = 0$ (perfect weak-anchoring) in some detail. First of all, it should be noted that the governing equations for this case are mathematically identical to those for a homogeneously aligned cell having the thickness $2d$; the boundary conditions, Eq. (6), are automatically satisfied owing to the symmetry of the problem. As a result, any expression obtained for a homogeneous cell of thickness $2d$ can be readily rewritten into the corresponding equation for the perfect weak-anchoring case by the following replacements: $\theta \to \theta$, $x \to x$, $V \to 2V$, $\delta \to 2\delta$. More generally, Eqs. (5)–(8) show that the same equation can be reached from the corresponding equation for a homogeneous cell of thickness d_h by $\theta \to \theta$, $x \to xd_h/2d$, $V \to 2V$, $\delta \to \delta d_h/d$. The appearance of a threshold voltage for $E_a = 0$ in Figure 5 is an immediate result of this fact and actually the threshold voltage equals 1/2 of that for a homogeneous cell. The elastic deformations in an electric field for homogeneously oriented cells were thoroughly studied by Gruler and co-workers.[16] Following their analysis, we can write down the phase difference, δ, and the voltage, V, in terms of θ_i for the perfect weak-anchoring case. Neglecting higher order terms in $\sin\theta_i$, we obtain

$$V = V_{\text{th}}\left\{1 + \frac{1}{4}\left(\frac{\Delta\epsilon}{\epsilon_2} + \frac{K_3}{K_1}\right)\sin^2\theta_i\right\}, \tag{9}$$

$$r_h \equiv 1 - \frac{\delta}{\delta_h} = \frac{n_e d}{4\lambda\delta_h}\nu\sin^2\theta_i\left\{1 + \frac{1}{8}\left(\frac{\Delta\epsilon}{\epsilon_2} + \frac{K_3}{K_1} - \frac{9}{2}\nu\right)\sin^2\theta_i\right\}, \tag{10}$$

$$\delta_h = d(n_e - n_o)/\lambda, \qquad \nu = \left(n_e^2 - n_o^2\right)/n_o^2,$$

$$V_{\text{th}} = \frac{\pi}{2}\left(\frac{K_1}{\epsilon_0\Delta\epsilon}\right)^{1/2}. \tag{11}$$

Here, V_{th} is the threshold voltage. These equations are of course valid at the intersection point ($V = V_t$, $\theta_i = \theta_t$). We can solve above equations for $\sin^2\theta_t$ in the following approximate form;

$$\sin^2\theta_t \simeq 2r_{hi}\left(\frac{V_{\text{th}}}{V_t}\right)^{1/2}\left\{1 + \frac{3\lambda\delta_h}{2n_o d}\left(\frac{3}{2}r_{hi} - 1\right)\right\},$$

$$r_{hi} = r_h|_{V=V_t}. \tag{12}$$

It should be emphasized that once the r_h vs V curves such as those shown in Figure 5 are obtained, the right-hand side of this equation can be calculated with sufficient accuracy. This is the central result of this section.

Now we return to the real system described in the last section. As the temperature approaches the lower boundary of the coexistence region, T_n, on cooling, the thickness of the isotropic phase, d_i, decreases and vanishes at T_n. Consequently, the evaporated SiO layer, getting in direct contact with the nematic liquid, turns to align the liquid crystal molecules homogeneously. By observing, at this point, the optical phase difference as a function of voltage, we can deduce one of the ingredients for the tilt angle determination, r_h vs V curve for the perfect weak-anchoring case; this can be done by reading $1/2$ of the actual voltage as "V" while keeping the phase difference unaltered. Another ingredient, r_h vs V curve for the nematic layer having the nematic–isotropic interface, can be obtained by extrapolating the optical phase difference observed in the coexistence region to T_n where the isotropic phase disappears. This manipulation is necessary because we can not measure the phase difference as a direct function of the voltage across the nematic layer due to the presence of the overlying isotropic liquid. Taking into account the voltage across the isotropic layer, we can write the total voltage as

$$V = \frac{D_x d_n}{\epsilon_2 \epsilon_0}\left\{\frac{1}{d_n}\int_0^{d_n}\left(1 + \frac{\Delta\epsilon}{\epsilon_2}\sin^2\theta\right)^{-1} dx + \frac{\epsilon_2}{\epsilon_i}\left(\frac{d}{d_n} - 1\right)\right\},$$
$$d = d_n + d_i \tag{13}$$

where ϵ_i is the dielectric constant of the isotropic phase and d_n stands for the nematic layer thickness. Now, we consider the total voltage as a function of the zero-field phase difference at temperature T, $\delta_0(T)$, and the relative decrease of δ from $\delta_0(T)$, $r_0 = 1 - \delta/\delta_0(T)$. If the perfectly strong or weak anchoring condition prevails at the nematic–isotropic interface, Eqs. (5)–(8) show that for fixed r_0, the voltage across the nematic layer becomes independent of the layer thickness. Therefore, considering Eqs. (8) and (13), we can show that the total voltage, $V(r_0, \delta(T))$, depends linearly on $1/d_n$, provided the material parameters are assumed to be unchanged. On the same ground, $\delta_0(T)$ can be shown to be proportional to d_n. As a result, by plotting $V(r_0, \delta_0(T))$ against $1/\delta_0(T)$, we obtain a set of straight lines each corresponding to a certain value of r_0. By extending these lines to $1/\delta_0(T_n)$, we can determine the voltage which gives rise to the relative

decrease, r_0, at the lower boundary of the coexistence region. It was also verified numerically that even for moderate anchoring conditions, this procedure gives a fairly accurate value for the voltage.

Finally, let us consider the relationship between the anchoring energy and the electric field-induced deformations. The anchoring energy is a measure which shows how steeply $F(\theta_i, \theta_t)$ increases around $\theta_i = \theta_t$. Thus it can be most simply defined by the second derivative of $F(\theta_i, \theta_t)$ at this point. For example, if we assume a widely used functional form for the interfacial free energy, $\frac{1}{2}E_a\sin^2(\theta_i - \theta_t)$, the anchoring energy is given by E_a. As shown in Figure 5, r_h increases more rapidly around $V = V_t$ as the anchoring becomes weaker. More generally, in the case of $d_i = 0$, we can obtain after a bit lengthy calculation a relation between the anchoring energy and the slope of r_h vs V curve at the intersection;

$$\frac{dE_a}{K_1} = \left(\frac{dV}{d\theta_i}\right)_w \frac{\pi\xi \sin\theta_t \cos\theta_t}{2V_{\text{th}}\left(1 + \dfrac{\Delta\epsilon}{\epsilon_2}\sin^2\theta_t\right)} \frac{\left(\dfrac{dr_h}{dV}\right)_w - \dfrac{dr_h}{dV}}{\dfrac{dr_h}{dV} - \left(\dfrac{dr_h}{dV}\right)_s},$$

$$E_a \equiv d^2F(\theta_i, \theta_t)/d\theta_i^2, \qquad \text{at } V = V_t, \theta_i = \theta_t \tag{14}$$

where

$$\left(\frac{dr_h}{dV}\right)_s = \frac{\pi}{2V_{\text{th}}\xi}\left(1 + \frac{\Delta\epsilon}{\epsilon_2}\sin^2\theta_t\right)\left(\frac{n_e - n_{ef}(\theta_t)}{n_e - n_o} - r_{hi}\right)$$

$$\xi = \int_0^{\theta_t}\left\{\frac{\left(1 + \dfrac{\Delta\epsilon}{\epsilon_2}\sin^2\theta_t\right)\left(1 + \dfrac{\Delta\epsilon}{\epsilon_2}\sin^2\theta\right)\left(1 + \dfrac{K_3 - K_1}{K_1}\sin^2\theta\right)}{\sin^2\theta_t - \sin^2\theta}\right\}^{1/2} d\theta$$

The subscripts, w and s, denote respectively that the derivatives must be taken along the r_h vs V curves for the perfect weak-anchoring and the perfect strong-anchoring conditions. Using the approximate expressions for r_h and V, Eqs. (9) and (10), above equations can be rewritten into a more transparent form.

$$\frac{dE_a}{K_1} \simeq \frac{\pi^2}{8}\left(\frac{\Delta\epsilon}{\epsilon_2} + \frac{K_3}{K_1}\right)\sin^2\theta_t\cos^2\theta_t \frac{\left(\dfrac{dr_h}{dV}\right)_w - \dfrac{dr_h}{dV}}{\dfrac{dr_h}{dV} - \left(\dfrac{dr_h}{dV}\right)_s}, \tag{15}$$

$$\left(\frac{dr_h}{dV}\right)_s \simeq \frac{r_{hi}}{V_t}. \tag{16}$$

Equation (16) offers a very simple way to find the slope of r_h vs V curve for the perfect strong-anchoring case: Draw a straight line through the origin and the intersection, and equate its slope with that in question. The validity of this procedure can be readily appreciated in Figure 5. Now that dr_h/dV, $(dr_h/dV)_w$, and $(dr_h/dV)_s$ are all experimentally accessible, we can in principle obtain the anchoring energy from Eq. (15). However, we must bear in mind that the use of this equation is effective only when these slopes differ appreciably from each other. In other words, the anchoring energy can be determined accurately from the electric field-induced deformations, only when the ratio, dE_a/K_1, between the extrapolation length and the nematic layer thickness is of order unity.

IV. RESULTS AND DISCUSSION

To examine the anchoring condition at the nematic–rubbed PVA interface, we have made 44-μm-thick and 12-μm-thick homogeneous

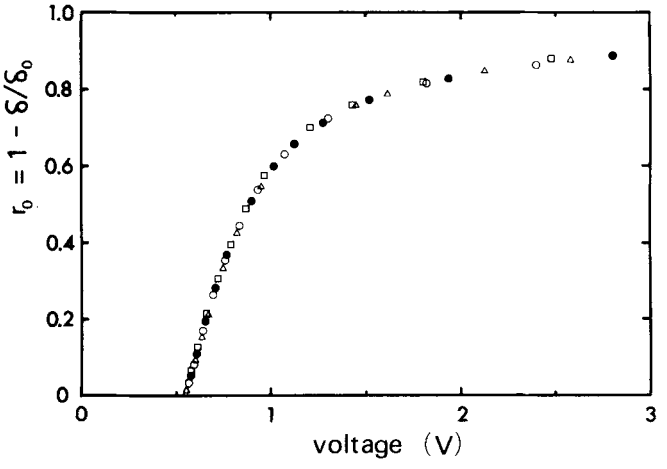

FIGURE 6 Voltage dependence of the relative decrease of the optical phase difference for various homogeneously aligned cells. (●): 44-μm-thick rubbed PVA–rubbed PVA cell filled with 2.6 mol% mixture (30.20 °C). (○): 12-μm-thick rubed PVA–rubbed PVA cell filled with 2.6 mol% mixture (30.20 °C). (□): 44-μm-thick rubbed PVA–rubbed PVA cell filled with pure 5CB (35.3 °C). (△): 43-μm-thick rubbed PVA–evaporated SiO cell filled with 2.6 mol% mixture (30.15 °C).

cells only using rubbed PVA coated substrates. These cells were filled with 2.6 mol% mixture of $C_6(CH_3)_6$/5CB. The optical phase differences were measured just below T_n ($= 30.20\,^\circ C$) as a function of voltage (325 Hz). The relative decrease, r_0 ($= r_h$), are shown in Figure 6. A threshold can be clearly seen for both cells, and moreover the whole voltage dependences agree quite well. This indicates unambiguously that as far as a nematic slab thicker than 10 μm or so is concerned, we can safely assume strong homogeneous anchoring for

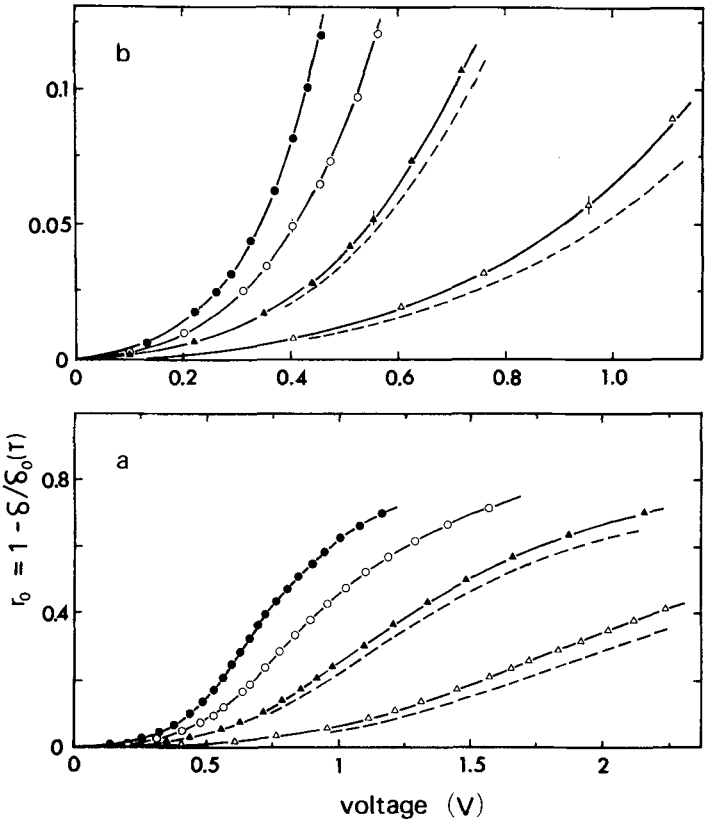

FIGURE 7 Voltage dependence of the relative decrease of the optical phase difference observed in the coexistence region. (b) shows the details of the small relative decrease part of (a). (△): $T = 30.58\,^\circ C$, $\delta_0(T) = 2.121 \pm 0.001$. (▲): $T = 30.46\,^\circ C$, $\delta_0(T) = 3.776 \pm 0.002$. (○): $T = 30.35\,^\circ C$, $\delta_0(T) = 5.258 \pm 0.002$. (●): $T = 30.23\,^\circ C$, $\delta_0(T) = 6.666 \pm 0.003$. Solid lines were calculated with $\theta_t = 0.49$ and $E_a = 2 \times 10^{-3}$ erg/cm^2. Dashed lines were calculated with $\theta_t = 0.49$ and $E = 10^{-2}$ erg/cm^2; to avoid complexity results for (△) and (▲) are shown. $F(\theta_i, \theta_t) = \frac{1}{2}E_a \sin^2(\theta_i - \theta_t)$ was assumed in the calculation. Voltage: AC 325 Hz.

the nematic–rubbed PVA interface. For comparison, the relative change of the phase difference for 44-μm-thick homogeneous cell filled with pure 5CB is included also in good agreement with the results for the mixture; observed just below T_c. This confirms, at least qualitatively, the fact that the properties of a nematic liquid crystal are approximately independent of the position in the nematic–isotropic coexistence region.

The optical phase difference for the nematic layer having the nematic–isotropic interface was observed at four distinct temperatures in the coexistence region. The relative decrease, r_0, are shown in Figure 7 as a function of the total voltage applied across the cell. It should be noticed here that the phase difference decreases continuously with the voltage, showing no threshold behavior. This shows, apart from the gap in the phase difference shown in Figure 3, the presence of the director tilt at the nematic–isotropic interface. The optical phase difference for the nematic layer homogeneously aligned on cooling between the evaporated SiO and the rubbed PVA substrates was measured just below T_n ($= 30.15\,^\circ$C). The results are shown in Figure 6 and are in good agreement with the results for other homogeneously aligned samples.

To obtain the tilt angle quantitatively, the relative decrease in Figure 7 was extrapolated to T_n according to the procedure described in the last section. The zero-field phase difference at T_n, 7.58, was used as determined in Section II. Examples of the extrapolation are shown in Figure 8. The resulted r_h's are shown in Figure 9 together with the r_h vs V curve for the perfect weak-anchoring condition deduced from the results given in Figure 6. The two curves intersect at $r_h = 0.128$ and $V_t = 0.31$ V while the threshold voltage, V_{th}, is 0.27 V. Using Eq. (12) we can obtain the tilt angle;

$$\theta_t = 0.49 \pm 0.01 \text{ rad} = 28.1 \pm 0.6\,^\circ.$$

We have taken account only of the experimental uncertainty and assumed $n_o = 1.555$ as a plausible value.[17]

Let us now proceed to determine the anchoring energy with the aid of Eqs. (15) and (16). By drawing a straight line in Figure 9 passing through the origin and the intersection, we can readily see

$$\frac{dr_h}{dV} \sim \left(\frac{dr_h}{dV}\right)_s \qquad \text{at } V = V_t.$$

When this happens, the anchoring energy can no longer be calculated accurately from Eq. (15). As a result, we must be satisfied only with

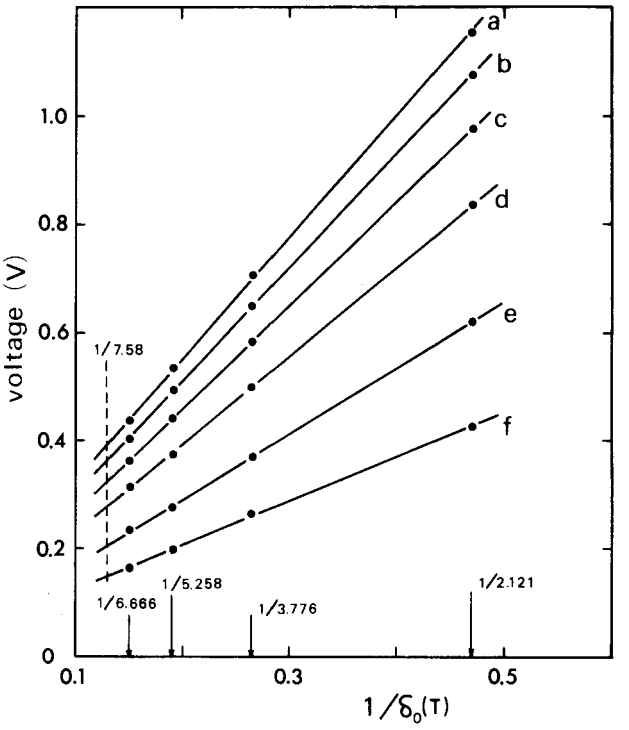

FIGURE 8 Examples of extrapolation procedure: a: $r_0 = 0.1$, b: $r_0 = 0.08$, c: $r_0 = 0.06$, d: $r_0 = 0.04$, e: $r_0 = 0.02$, f: $r_0 = 0.01$.

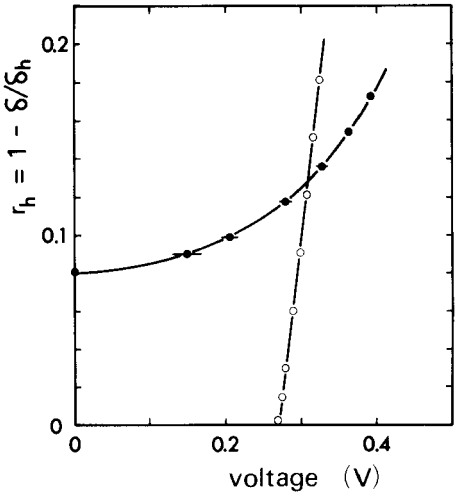

FIGURE 9 Deduced r_h vs V curves for imaginary 43-μm-thick nematic films having either the perfect weak-anchoring boundary (○) or the nematic-isotropic interface (●). $\delta_h = 8.25$.

placing a lower bound to the anchoring energy;

$$dE_a/K_1 > 20 \qquad (\text{or } E_a > 10^{-3} \text{ erg/cm}^2, \text{ see below}).$$

Substituting $d = 43$ μm we can conclude that the extrapolation length, K_1/E_a, is less than about 2 μm. To take a closer look at the anchoring energy, we must deal with the results for thinner nematic films in which the anchoring effect can be more pronounced. In order to make numerical calculations regarding E_a as an adjustable parameter, we measured, first of all, the dielectric constants separately at 325 Hz;

$$\epsilon_1 = 16.2 \pm 0.1, \qquad \epsilon_2 = 8.2 \pm 0.1, \qquad \epsilon_i = 10.9 \pm 0.1.$$

These values are in reasonable agreement with those reported in the literature.[18] Using these in Eq. (11) we obtain the splay elastic constant,

$$K_1 = 2.1 \times 10^{-7} \text{ dyn.}$$

The bend elastic constant was determined to give the best fit to the results shown in Figure 6;

$$K_3 = 2.8 \times 10^{-7} \text{ dyn.}$$

The solid lines in Figure 7 were calculated numerically by using the relevant parameters obtained above. The anchoring energy was assumed to be 2×10^{-3} erg/cm^2. It can be clearly seen that the experimental points are reproduced quite well all through the voltage range of measurement, showing the validity of the value for the tilt angle. For comparison, the dashed lines were calculated with $E_a = 10^{-2}$ erg/cm^2 for two thinner preparations. Apparently, the dashed lines deviate considerably from the experimental results. However, if we consider, for instance, the dielectric constant of the isotropic phase, ϵ_i, as an adjustable parameter, a good agreement can be reached between the theoretical and experimental results by assuming $\epsilon_i = 12.0$, although this value seems too large compared with the measured value as well as the mean dielectric constant. So, in order to extract an unequivocal value for the anchoring energy from the numerical analysis, a great care should be taken concerning the material parameters. In view of these facts, it might be safe, here, to conclude that the anchoring energy is of the order of 10^{-3} erg/cm^2.

So far we have considered the nematic–isotropic interface as an ideally flat interface, and hence neglected the deviations from planarity caused by the electric field. When the field is weak, the contribution of the interfacial tension will dominate and thus the planar interface might be favored. In fact, we did not observed any distortion under a microscope when the field was so limited that the relative decrease of phase difference, r_0, did not exceed 0.7. In this case, the initially observed zero-field phase difference was instantaneously regained when the field was removed. However, at higher voltages the interface deformed into an undulated structure which could be seen between crossed polarizers as parallel stripes mostly along the rubbing direction. The width of the stripes was about a few hundred micrometers. This distortion shares several common features with the deformation of a free surface of a nematic liquid in the presence of a magnetic field predicted by de Gennes;[19] free from stationary hydrodynamic motions, essentially independent of the driving frequency, etc. A detailed study is now under way and will be reported elsewhere. In any case, the high field instability presents no serious problem for the present purpose, because only the behavior at low voltages is important here.

Finally we would like to discuss briefly the origin of the tilt angle at the interface. The orientation at the nematic–isotropic interface was first studied theoretically by de Gennes[1] in terms of the anisotropy of the spacial variations of the order parameter. He showed that the interfacial free energy can be minimized only when the director is parallel or perpendicular to the interface, provided the director is assumed to be uniform in space. More generally it can be easily shown that this result remains true even when the director is allowed to vary in space as long as the uniaxial symmetry is assumed.[20] Therefore, it seems at present somewhat difficult to explain the occurrence of the tilted orientation only with the Landau-de Gennes theory, though it gives a good estimate for the interfacial tensions. The Landau-de Gennes theory is based on expanding the Landau free energy with respect to the quadrupolar tensor order parameter and its spatial derivatives. Strictly speaking, the gradient expansion is valid only when the order parameter varies slowly over the range of molecular interaction, which is evidently no longer true in the case of the nematic–isotropic interface. So it is not surprising even if the theory fails to predict the interfacial tilt.

The tilted orientation is also known to occur at the free surface of a nematic liquid crystal.[21] Parsons[22] attributed this to the existence of a

highly polar end group on the molecule which tends to point to the bulk of the liquid crystal which is more polar than the vapor phase. Cyanobiphenyls have a large dipole moment along the long axis of the molecule. In fact, 5CB has been observed to orient perpendicular to the free surface.[23,24] Similarly, at the nematic–isotropic interface, we can expect that the polar interaction will tend to align the molecules perpendicular to the interface. If the quadrupolar interaction, which has been thought to be mainly responsible for the nematic order, has a tendency to align the molecules parallel to the interface, we can expect that the competition between the polar and the quadrupolar contributions will give rise to the tilted orientation. The strength of the polar effect is of course strongly dependent on the microscopic structures of the nematic and isotropic phases. In particular, the antiferroelectric short range order proposed by several authors[25,26] for cyanobiphenyls may have a significant effect on the interfacial orientation of the liquid crystal.

V. CONCLUSION

We have prepared a flat and stable nematic–isotropic interface in an equilibrium condition for 5CB mixed with a small amount of $C_6(CH_3)_6$. The preparation method is based on the fact that if the substrates of a sandwich-type cell are treated in such a way that the nematic phase wets preferentially one of the substrates while the isotropic phase wets the other, the equilibrium configuration of the coexisting nematic and isotropic phases may be a stratified structure with their interface parallel to the substrates. Therefore, this method has an advantage that the interface can be obtained in a conventional sandwich-type cell of a few tens of micrometers thick with well defined director orientation. As a result, this system can be quite useful for the study of various properties of the nematic–isotropic interface such as the interfacial tension, the orientation of the director at the interface, the light reflection and scattering from the interface, and their response to external fields. As an example, we have attempted to determine the director orientation at the interface from the observations of the electric field-induced deformations in the nematic layer. For this purpose, a simple procedure which requires little knowledge about the material parameters was developed. For 2.6 mol% mixture of $C_6(CH_3)_6$/5CB, the director was found to be tilted by $28.1 \pm 0.6°$ from the interface. In addition, the anchoring energy at the interface was also estimated to be on the order of 10^{-3} erg/cm^2.

Using these values, we could satisfactorily reproduce the experimental results. Since the surface treatments employed here, coating with rubbed PVA film and oblique evaporation of SiO, have quite a universal capability to orient liquid crystal molecules, the present technique might also be applicable to wider range of materials.

References

1. P. G. de Gennes, *Mol. Cryst. Liq. Cryst.*, **12**, 193 (1971).
2. R. B. Meyer, *Mol. Cryst. Liq. Cryst.*, **16**, 355 (1972).
3. D. Langevin and M. A. Bouchiat, *Mol. Cryst. Liq. Cryst.*, **22**, 317 (1973).
4. R. Williams, *Mol. Cryst. Liq. Cryst.*, **35**, 349 (1976).
5. P. Sheng and E. B. Priestley, in *Introduction to Liquid Crystals*, edited by E. B. Priestley, P. J. Wojtowicz and P. Sheng, Plenum, New York (1975).
6. R. Vilanove, E. Guyon, C. Mitescu and P. Pieranski, *J. Physique*, **35**, 153 (1974).
7. H. Yokoyama, S. Kobayashi and H. Kamei, *Appl. Phys. Lett.*, **41**, 438 (1982).
8. H. Yokoyama, S. Kobayashi and H. Kamei, in *Proceedings of the Ninth International Liquid Crystal Conference*, Bangalore, December 1982; *Mol. Cryst. Liq. Cryst.*, **99**, 39 (1983).
9. L. D. Landau and E. M. Lifshitz, *Statistical Physics*, Pergamon, Oxford (1970).
10. D. E. Martire, in *The Molecular Physics of Liquid Crystals*, edited by G. R. Luckhurst and G. W. Gray, Academic, London (1979).
11. D. H. Chen and G. R. Luckhurst, *Trans. Faraday Soc.*, 65, 656 (1969); B. Kronberg, D. F. R. Gilson and D. Patterson, *J. Chem. Soc., Faraday* II, **72**, 1673 (1976).
12. T. W. Stinson and J. D. Litster, *Phys. Rev. Lett.*, **25**, 503 (1970); **30**, 688 (1973).
13. H. Yokoyama, S. Kobayashi and H. Kamei, *Rev. Sci. Instrum.*, **54**, 611 (1983).
14. D. Meyerhofer, *Phys. Lett.*, **51A**, 407 (1975).
15. S. Naemura, *Appl. Phys. Lett.*, **33** 1, (1978).
16. H. Gruler, T. J. Scheffer and G. Meier, *Z. Naturforsch*, **27A**, 966 (1972).
17. P. P. Karat and N. V. Madhusudana, *Mol. Cryst. Liq. Cryst.*, **36**, 51 (1976).
18. P. G. Cummins, D. A. Dunmur and D. A. Laidler, *Mol. Cryst. Liq. Cryst.*, **30**, 109 (1975).
19. P. G. de Gennes, *Solid State Commun.*, **8**, 213 (1970).
20. H. Yokoyama, (unpublished).
21. M. A. Bouchiat and D. Langevin, *Phys. Lett.*, **34A**, 331 (1971).
22. J. D. Parsons, *Phys. Rev. Lett.*, **41**, 877 (1978); *Mol. Phys.*, **42**, 951 (1981).
23. M. Gannon and T. E. Faber, *Philos. Mag. A*, **37**, 117 (1978).
24. D. Beaglehole, *Mol. Cryst. Liq. Cryst.*, **89**, 319 (1982).
25. A. J. Leadbetter, R. M. Richardson and C. N. Colling, *J. Physique*, **36**, C1-37 (1975).
26. J. E. Lydon and C. J. Coakley, *J. Physique*, **36**, C1-45 (1975).